COUPLING OF WALL BOILING WITH DISCRETE POPULATION BALANCE MODEL

C. Lifante¹, F. Reiterer¹, Th. Frank¹ and A. Burns²

ANSYS Germany GmbH, Otterfing, Germany

ANSYS UK, Milton Park, Oxforshire, UK

conxita.lifante@ansys.com

Abstract

A coupling between a polydisperse population balance method (Multiple Size Group Model - MUSIG) and the RPI wall boiling model for nucleate subcooled boiling has been implemented in ANSYS CFX. It allows more accurate prediction of the interfacial area density for mass, momentum and energy transfer between phases in comparison to the usual local-monodisperse bubble size assumption and underlying bulk bubble diameter correlations as they are commonly used in boiling flow applications like e.g. the prediction of subcooled nucleate boiling in rod bundles and fuel assemblies of PWR. The paper outlines the methodology of the coupled CFD model, which automatically avoids possible inconsistencies in the model formulation for the heated wall, when the generated steam bubbles on the heater surface are injected exactly in the bubble size class corresponding to the predicted bubble departure diameter.

The coupling of the RPI wall boiling model and the MUSIG model has been implemented for both homogenous/inhomogeneous variants of the MUSIG model. The paper presents the validation of the coupled modeling approach for the well known test case of nucleate subcooled boiling of R113 refrigerant in a circular annulus with inner heated rod based on the experiments of Roy et al. [1]. ANSYS CFX results with the newly implemented approach as well as comparison to data and locally-monodisperse simulations are provided.

1. Introduction

Subcooled boiling is present in many industrial applications. Among them we can find the simulation of flows in the primary cooling system of nuclear reactors. For instance, the accurate prediction of temperature distribution and gas volume fraction around fuel rod bundle is of main importance in order to improve designs or analyze suitable failure scenarios. Some of the current CFD codes simulate wall boiling by means of the so-called RPI or wall heat flux partitioning model. In this model, a number of sub-models of the overall mechanistic model were taken from correlations originally developed for use in one-dimensional thermo-hydraulic simulation methods and system codes. One of those correlations predicts the local mean bubble diameter within in the bulk sub-cooled fluid flow in dependence on local liquid sub-cooling temperature. Commonly the correlation by Kurul & Podowski [2]s used to evaluate this quantity, which in turn affects through calculated interfacial area density all mass, momentum and heat transfer processes. However such an approximation shows two main deficiencies. The first one is the decoupling of this value from the bubble diameter at bubble departure from the heated wall. If no consistent correlations for both bubble diameters are used, a discontinuity of the bubble diameter near the wall may appear with resulting negative consequences for the accuracy and convergence of the CFD solver. The second disadvantage is the fact that such correlations provide locally one single value, i.e. this is a locally-monodisperse approach. In wall boiling simulations, like in any other multiphase application, the proper prediction of the interfacial area density is crucial, and it depends on the size of the bubbles present in the domain. Therefore, the simulation of a spectrum of bubbles, instead of one single bubble size, reproduces more accurately the multiphase flow morphology and the interphase transfer phenomena.

To avoid those issues and in order to increase the accuracy and predictive capability of the model a coupling between the RPI wall boiling model and a population balance approach (MUSIG – Multiple Size Group Model) has been derived and implemented into a customized version of ANSYS CFX 12.1, generalizing the approach by Tu & Yeoh [3] to inhomogeneous MUSIG to better account for the different behavior of different bubble size classes. The MUSIG model assumes that bubbles of different sizes may be present in the flow and for each bubble size class a so-called size fraction equation is solved. This is in fact a mass conservation equation of each discrete class of bubbles. In addition, the bubbles may share the velocity field (homogeneous MUSIG) or move with their own velocity (inhomogeneous MUSIG [4]). It is well known that small and large bubbles behave significantly different, and one single velocity field for a wider spectrum of bubble size classes can lead to inaccuracies in the predicted results. The coupling of the MUSIG model to the wall boiling model as described here has been implemented for both MUSIG approaches. The evaporation rate as computed by the RPI wall boiling model has been introduced as a source term in the size fraction equation of the bubble class, whose corresponding diameter is the closest to the bubble departure diameter.

2. Mathematical Model Formulation

2.1 The RPI Wall Boiling Model

The model formulation which is provided here deals with the physical-mathematical description of the wall-bound evaporation processes during nucleate subcooled boiling, i.e. boiling on a heated surface with significant applied heating power, where the fluid temperature in the core flow is still significantly below the saturation temperature of the fluid. After the onset of nucleate boiling this kind of flow results in a dispersed bubbly steam-fluid flow with rapidly increasing steam volume fraction. It is clear that detailed physics of bubble growth is very complex, and occur on very small length scales in the vicinity of the wall. It is unrealistic to model the detailed physics in a phase-averaged Eulerian multi-phase model or to resolve the small length scales with ultra-fine meshes. Therefore a so-called mechanistic model has been chosen to model the wall boiling phenomena. It aims to model the important and non-resolved physical sub-processes by using engineering correlations. This model is a sub-grid scale model in the sense that the complex physics is assumed to take place in vicinity very close to the wall which is smaller than the mesh resolution at the heated surface. In the RPI wall boiling model requires quite a number of correlations or sub-models, where most of them come initially from applications in one-dimensional thermohydraulic modelling or system codes.

The RPI wall boiling model assumes that the total heat flux applied on a heated wall is transferred into the fluid domain through different mechanisms: i.e. convection to the continuous phase, the conduction to the continuous phase when bubbles detach the wall and fresh liquid gets in contact with the heated wall (this process is also known as quenching), and due to the

evaporation of the fluid. The algorithm of the RPI wall boiling model searches for solution of the non-linear equation in terms of T_w , which fulfils the heat flux partitioning:

$$Q_{w} = Q_{conv}(T_{w}) + Q_{auench}(T_{w}) + Q_{evap}(T_{w})$$

$$\tag{1}$$

Individual terms in eq. (1) are evaluated based on the mentioned sub-models and correlations (see [5], [6]). Two of the model parameters are the bulk bubble diameter (d_B) and the bubble departure diameter (d_w). In the traditional modelling approach of the RPI wall boiling model each of them is computed through an independent correlation. Usual applied methods for the evaluation of d_B are correlations as the one by Kurul & Podowski [2]. In this case the bubble diameter is computed as follows

$$d_{B} = \begin{cases} d_{0} & \Delta T_{sub} > \Delta T_{0} \\ \frac{d_{1}(\Delta T_{sub} - \Delta T_{0}) + d_{0}(\Delta T_{1} - \Delta T_{sub})}{\Delta T_{1} - \Delta T_{0}} & \Delta T_{1} < \Delta T_{sub} < \Delta T_{0} \\ d_{1} & \Delta T_{sub} < \Delta T_{1} \end{cases}$$

$$(2)$$

Where standard parameter values are $d_0 = 0.15$ mm, $d_1 = 2$ mm, $\Delta T_0 = 13.5$ K and $\Delta T_1 = -5$ K. Such simplified models provide one single value at any location of the fluid domain, assuming that there is locally only one kind of bubbles.

Further a commonly used formulation for the computation of the bubble departure diameter d_w is the correlation by Tolubinsky & Kostanchuck [7]:

$$d_{w} = \min(d_{ref} \cdot e^{\frac{-\Delta T_{sub}}{\Delta T_{ref}}}, d_{max})$$
(3)

with typical model parameters being set to $d_{\max} = 1.4$ [mm], $d_{ref} = 0.6$ [mm] and $\Delta T_{ref} = 45$ [K]. The main drawback of applying two disconnected model formulations is the possible discontinuity in the radial distribution of the bubble diameter when we are approaching the heated wall. The limit of the bulk diameter towards the wall may not coincide with the locally predicted value of the bubble departure diameter.

2.2 The Population Balance Method (MUSIG Model)

The population balance methods are a family of models where the interfacial length scales of the disperse phase, i.e. the bubble diameters of a gas-liquid flow, are characterized not just by a single value but by the characterization of the bubble size distribution either with a PDF or by discretization in bubble size classes. In this way the corresponding mean Sauter diameter and the interfacial area concentration can be evaluated more accurately. The way in which the particle spectrum is computed differs from one to the other method. For the current study the MUSIG model was chosen, which uses a discrete representation of the bubble size distribution by size fractions over a larger number of discrete bubble size classes.

The MUSIG model assumes that different kinds of bubbles (classes) are present in the domain and solves for each bubble class a transport equation. It represents a mass conservation equation

for the bubbles in the particular bubble size class (i). The MUSIG model can be categorized into two variants depending on the made assumptions about disperse phase velocity of the bubbles. If it is assumed that all bubbles share the same velocity, it is called the homogeneous MUSIG model. If, on the contrary, it is assumed, that bubbles of different size can move with different velocities, it is named inhomogeneous. In order not to solve a full set of Navier-Stokes equations for each individual bubble size class, the bubble size classes are split into groups in this case, where the bubbles belonging to such a group share the same velocity field (velocity group). An extra set of Navier-Stokes equations is then solved for each velocity group. This consideration can have substantial impact on the accuracy of the CFD simulations. It is known the unlike behaviour that small and large bubbles may present. For instance, small bubbles usually flow with the continuous phase while large bubbles are more influenced by buoyancy. Even the sign of the lift coefficient changes at a critical bubble diameter, which depends on the flow conditions and the Eötvos number. A common velocity for the whole disperse phase in such applications would lead to erroneous results.

The standard formulation of the MUSIG model equations in terms of the corresponding size fractions for a given bubble size class (*i*) look like

$$\frac{\partial}{\partial t} (\rho_{i} r_{d} f_{i}) + \frac{\partial}{\partial x^{j}} (\rho_{i} r_{d} U_{i}^{j} f_{i}) = B_{B_{i}} - D_{B_{i}} + B_{C_{i}} - D_{C_{i}} + S_{fci}$$
(4)

where the first four terms on the RHS correspond to the birth (B) and death (D) of (*i*)-class bubbles due to break up and coalescence processes. Usual formulation based on the models of Prince & Blanch [5] and Luo & Svendsen [5] are applied. The last source term corresponds to the nucleation, shrink and growth of bubbles when evaporation or condensation takes place. Underlying model formulation for the RHS terms were derived in collaboration between ANSYS and HZDR and further details can be found in [8].

2.3 Coupling between RPI Wall Boiling & MUSIG Model

In the present work it is assumed that the gaseous phase is always at saturation temperature and no overheated vapour is considered. The last term in the wall heat partitioning equation (1) corresponds to the wall heat flux component which leads to the evaporation of the liquid in the vicinity of the wall. It is computed as:

$$Q_{evap} = \dot{m}_{evap} \cdot h_{lg} \tag{5}$$

where \dot{m}_{evap} is the evaporation rate and h_{lg} is the latent heat of evaporation. The evaporation rate is modelled as:

$$\dot{m}_{evap} = \frac{\pi}{6} d_w^3 \rho_g fn \tag{6}$$

being ρ_g the density of the gaseous phase, f the bubble detachment frequency and n the nucleation site density. The last two parameters are likewise evaluated through correlations [5]. Now the coupling between the RPI wall boiling and the MUSIG model consists of a link between the vapour mass which is generated at the wall (and computed by the RPI wall boiling model) and the bubbles located near the wall, assuming that their dimension

corresponds exactly to the bubble departure diameter at the given position on the heated wall. This was implemented by including one more mass source term into eq. (4). However, the mass transfer term should only be activated for the size fraction equation which is corresponding to the bubble size class whose representative diameter is the closest to the bubble departure diameter. Since the evaporation rate, \dot{m}_{evap} , computed during the wall heat partitioning is an wall area specific value, it must be transformed into a volumetric source term in the near-wall mesh cell. ANSYS CFX performs this transformation by means of a multiplication by the ratio between the volume of the control volume (V) and its surface (S).

$$\dot{m}_{evap}^{V} = \dot{m}_{evap} \frac{V}{S} \tag{7}$$

The coupling has been implemented for both homogeneous and inhomogeneous MUSIG model variants. In the first case, it is required to identify at each time and position at the wall, which bubble size class (i.e. its representative bubble diameter) is the closest to the bubble departure diameter. Consequently this identifies into which size fraction equation the mass source term has to be included.

For the inhomogeneous case, in addition, it must be identified to which velocity group that bubble class belongs. Secondary momentum flux terms must be included into the Navier-Stokes equation corresponding to the determined velocity group. This has not to be taken into account for the homogeneous MUSIG because there is only one velocity group and therefore only one Navier-Stokes equation solved for the gaseous phase.

 $(R_i)(R_o)$

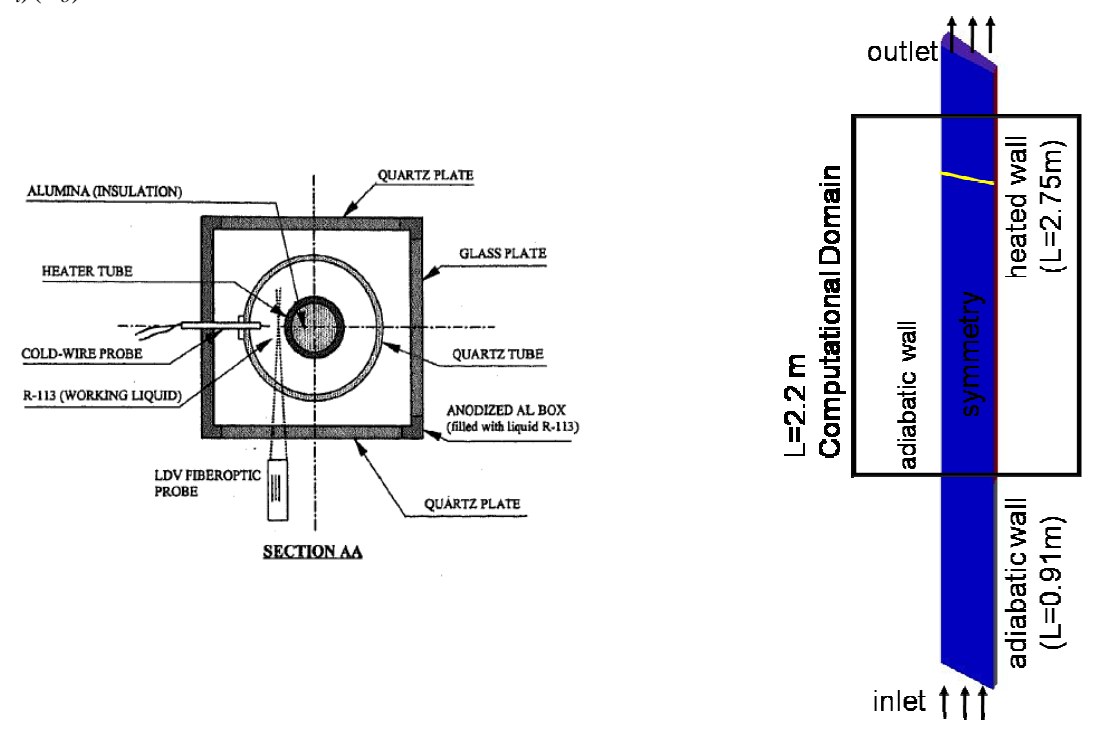


Figure 1. Left: Sketch of the experimental test facility. Right: Computational domain.

3. Validation Study

After the derivation of the coupled model formulation and its implementation in a customized solver version of ANSYS CFX 12.1 a validation study was performed in order to evaluate its appropriateness for the accurate prediction of wall boiling applications.

3.1 Test Case Description

In order to validate the coupling between the RPI wall boiling model and the population balance approach (here the inhomogeneous MUSIG model) an experiment by Roy et al. [1] performed at the Arizona State University was selected from the open scientific literature. The experiment consists of the upward flow of subcooled R-113 refrigerant in a vertical circular annulus with an inner radius of 7.89 mm, an outer radius of 19.01 mm and a length of the experimental test section of 3.66 m. The outer wall of the circular annulus is adiabatic and the inner wall is split into two regions: the first 0.91 m are adiabatic wall and the upper 2.75 m of the wall are homogeneously heated. The measurement devices were located at an elevation of 1.984 m inside the heated section, providing detailed flow information like vapour volume fraction, temperatures, velocities, turbulent kinetic energy and mean Sauter diameter. This makes the test especially suitable to validate the new methodology. A sketch of the experimental facility is included in Figure 1. In order to save computational time only a domain of 2.2 m was defined, considering exclusively a segment of the heated wall.

3.2 Numerical Simulations and Results

Different test conditions were studied by Roy et al. [1] at the experimental test facility. A number of these different test conditions had been studied in the present validation analysis. But because quite similar results could be obtained for all the different test conditions and the same drawn conclusions, detailed results for only one representative test case had been included in this work. In that case the pressure at the measurement plane was 2.69 bar, the mass flow rate was set to $784 \text{ kg/m}^2\text{s}$, the average liquid temperature at the channel inlet was 50.2 C and the inner wall heat flux was kept constant at 116KW/m^2 .

For the initialization of the fluid domain and the prescription of proper inlet boundary conditions the vertical upward flow of R-113 was first performed as a steady-state single-phase flow computation in order to obtain fully developed flow conditions for the circular annulus flow. Profile information for the fluid velocity components and turbulence properties had been extracted from the outlet cross section of that single-phase flow simulation and had subsequently been used for domain initialization and inlet boundary conditions for all following multiphase flow computations. The thermodynamic properties required for the CFD computation were introduced by means of a RGP¹ table, which was obtained from the *RefProp* database [9].

The simulation was carried out by applying a two-phase Eulerian model for the disperse multiphase flow mixture of liquid R-113 and its the steam phase, which was assumed to form a polydisperse disperse phase in the observed range of steam volume fractions. The CFD setup for

¹ RGP table – Real Gas Property table

the multiphase flow computation as completed by including Grace drag and FAD² turbulent dispersion force for the interfacial momentum exchange between the two phases.

Furthermore, turbulence of the continuous phase was modelled by the SST model [10]. The enhancement of turbulence as induced by the presence of bubbles under the influence of buoyancy was calculated following the approach of Morel et al. [11]. This model for bubble induced turbulence introduces an extra source term for the turbulent kinetic energy and the turbulent eddy dissipation which are derived in dependence on the bubble drag force. The heat transfer between phases was modelled by the Tomiyama correlation [12].

As found by Koncar & Krepper [13], the growing but initially still stationary steam bubbles at the surface of the heated wall influence the near wall fluid velocity profiles. As found by these authors this influence can be taken into account in a similar way as it is applied for the wall modelling of rough walls, where a wall roughness with a magnitude proportional to the bubble departure diameter is introduced. In the present computations the sand-grain coefficient in the fluid phase rough wall model was specified as:

$$k_r = \eta \cdot d_W \cdot \left(1 - \frac{Q_{conv} + Q_{quench}}{Q_W}\right)^{\zeta} = 0.575mm \tag{8}$$

where model parameters were set to $\eta = 0.5$ and $\zeta = 0.174$.

Bubble coalescence and break up phenomena were modelled by applying the standard Luo & Svendsen and Prince & Blanch models [5]. A parametric study of their factors was performed leading to the optimized values of zero for break up (switched off) and 4.0 for the turbulent coalescence coefficient. This indicates that the physical phenomena playing a main role in this application are the coalescence of bubbles near the wall and their re-condensation when they are in contact with the sub-cooled bulk liquid. The bubble departure diameter predicted in accordance to the eq. (3) usually shows only a minor variation along the heated wall surface in dependence on local flow conditions. But in order to exclude a possible influence of inaccurate results from the Tolubinski & Kostanchuk correlation [14] it was decided to use for the present investigation a constant bubble departure diameter, which was set from the experimental data to 1.3mm.

The MUSIG model was run with a discretization of the bubble diameter distribution into 15 different bubble size classes ranging from 0.25 to 3.75 mm. The minimum and maximum of bubble sizes was chosen in accordance to the experimental observations in order to allow for a maximum resolution in the given bubble diameter range. Furthermore the CFD simulations for the test case of Roy et al. could be carried out by choosing the homogeneous MUSIG model because the critical diameter with respect to the sign of the lift force coefficient was substantially larger than the upper limit of the chosen bubble size distribution for this application.

_

² FAD – Favre Averaged Drag

Table 1. Main characteristics of numerical meshes.

	Mesh 1	Mesh 2	Mesh 3	Mesh 4
Radial cells	8	16	32	64
Axial cells	220	440	880	1760
y max (single phase)	119	62	34	20

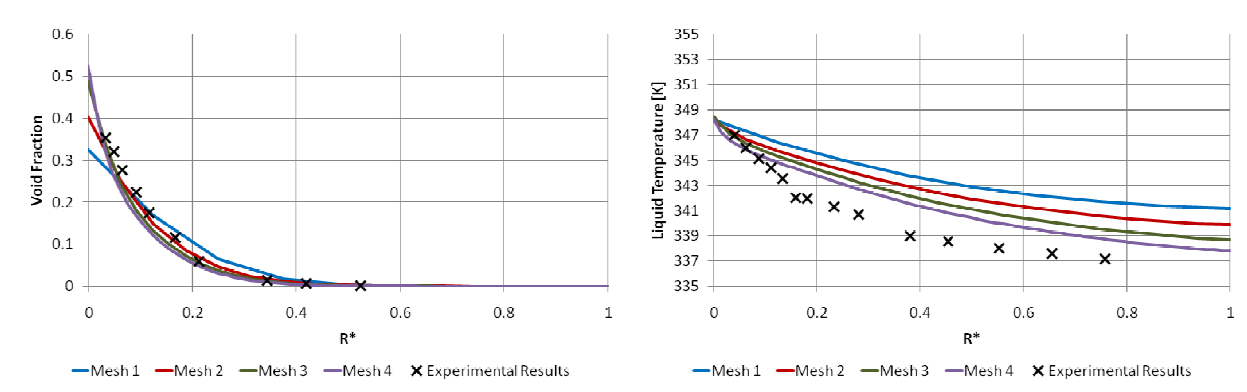


Figure 2. Grid independence study. Comparison of CFD solutions to experimental data [1] at measurement plane. Left: Steam volume fraction. Right: Liquid temperature.

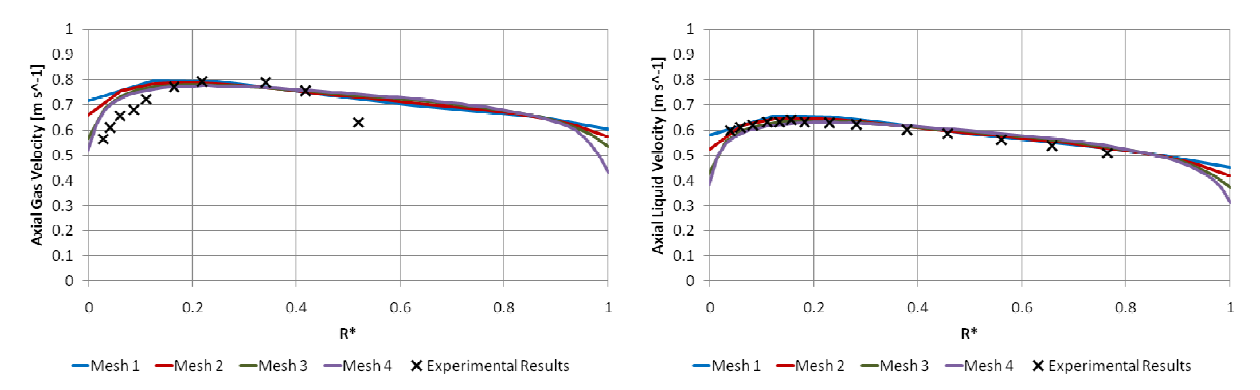


Figure 3. Grid independence study. Comparison of CFD solutions to experimental data [1] at measurement plane. Left: Axial steam velocity. Right: Axial liquid velocity.

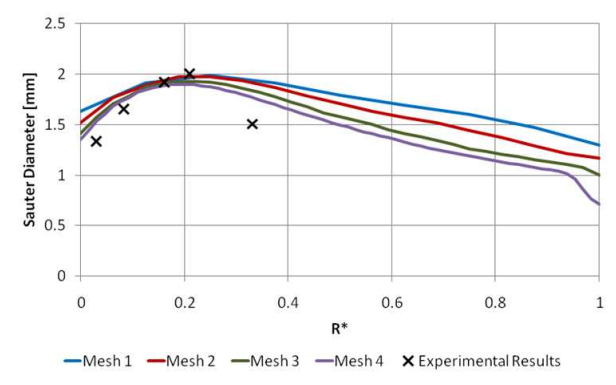


Figure 4. Grid independence study. Comparison of CFD solutions to experimental data [1] at measurement plane. Left: Mean Sauter Diameter.

3.2.1 Spatial Grid Independence Analysis

Following the Best Practice Guidelines [15] the boiling flow in the circular annulus was simulated on four different equidistant 2D grids consistently refined in each direction with a factor of two. The coarsest grid contains 1.760 cells and the finest grid had 112.640 cells. Main properties of the grids are summarized in Table 1. Due to the consideration of rough walls in the multiphase flow simulations, the resulting y^+ values in the turbulent wall treatment are clipped. To have a better imagination about the near wall resolution of the applied grids, the corresponding single-phase y^+ values are presented here. Its maximum value of y^+ ranges from 119 to 20.

Figures below show the results regarding the main characteristic variables of the boiling multiphase flow under consideration for the 4 CFD simulations on the hierarchically refined grids. The diagrams in Figure 2 , Figure 3 and Figure 4 correspond to radial distributions at the elevation of the measurement plane at L=1.984m downstream the inlet. A monotonic approximation towards the experimental results with grid refinement can be observed for the void fraction and the liquid temperature. Grid independent results can be observed already for the results corresponding to Mesh 3. The only deviation can be observed for the liquid temperature between the CFD solutions on the third and fourth grid. Even finer grids in radial direction would be required to reach completely grid independent results. This is unfortunately not possible with the current formulation of the RPI model. However this change in liquid temperature is smaller than 1 K. The same difference in temperature is observed in comparison to the experimental results. The coincidence of the predicted void fraction profile and the axial velocity profiles of both phases in comparison to the experimental data is quite remarkable. The behaviour of the Mean Sauter Diameter in the zone where gas is present (R^* =0...0.4) is analogous.

3.2.2 <u>Analysis of Independence from Bubble Size Class Discretization</u>

Since in the presented coupled simulation approach a discrete population balance approach is used (homogeneous MUSIG model), the CFD results might be not only influenced by the spatial discretization of the numerical mesh, but by the discretization of the bubble diameter space, i.e. the discretization of the bubble size distribution into discrete bubble size classes, as well. Therefore an analysis has been done to quantify the remaining discretization error with respect to the chosen number of bubble size classes in the MUSIG model. Based on Mesh 3 which has shown an almost grid independent CFD solution, further simulations had been carried out with different bubble diameter discretizations. In all investigated cases the bubble diameter range was kept constant with the defined range of [0.25mm-3.75 mm]. The number of classes was varied from 7, 15, 30 and finally up to 60 bubble size classes in the homogeneous MUSIG model.

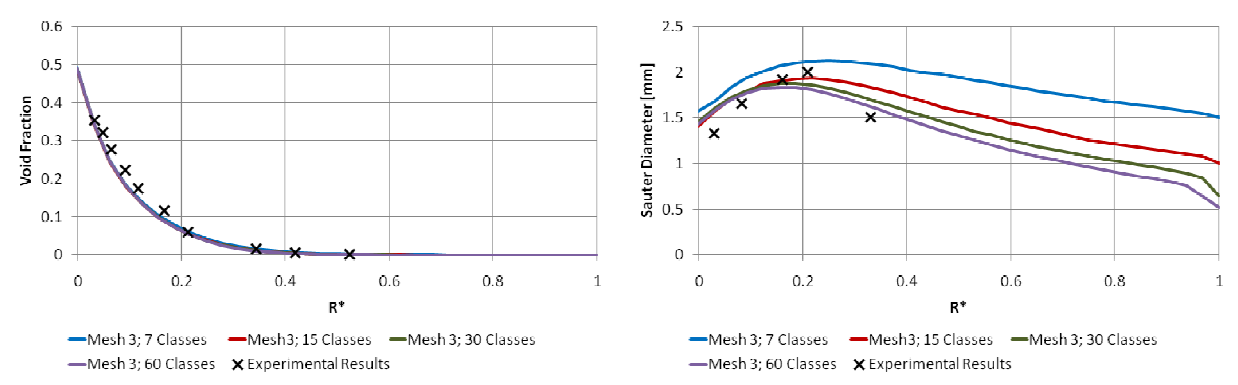


Figure 5. Investigation regarding independence of CFD solution from bubble size distribution discretization. Comparison of CFD results to experimental data [1] at the measurement plane. Left: Steam volume fraction. Right: Sauter mean diameter.

Figure 5 shows the result of the refinement regarding the number of bubble size classes. Again steam volume fraction and Sauter mean diameter profiles at the measurement plane were investigated. The radial distribution of the steam volume fraction (left) does not appear to be very sensitive to the increase of the number of bubble size classes. However, other variables like the Sauter mean diameter (right) show a strong influence of the chosen discretization. The CFD results get substantially closer to the experimental data with increasing number of bubble size classes and are in a much better agreement with them in comparison to results obtained with the traditional locally-monodispersed bubble diameter assumption. Independence from bubble size discretization can be achieved with about 25-30 bubble size classes in the MUSIG model if we focus on the fluid domain area where a significant amount of steam is present ($R^*=[0, 0.4]$,

being R^* the dimensionless radius based on the outer and inner radius $R^* = \frac{R - R_i}{R_o - R_i}$; even the last

available measurement point at R*=0.35 has to be regarded as of questionable measurement accuracy due to lack of steam).

At the measurement plane elevation two monitor points were defined in the CFD simulation: Point 1 is located at the radial dimensionless position of R*=0.03, which is situated very close to the heated wall; and Point 2 at R*=0.16, whose location is shifted towards the centre of the pipe,

but still in the sensible area of the near wall steam layer. At those two points, the whole bubble diameter spectrum has been analyzed. At both locations (Figure 6) the effect of a too coarse bubble size class resolution is clearly detected. Nevertheless the profiles of bubble size distributions in Figure 6 are monotonically converging. At the first point (left diagram), a maximum close to a bubble diameter of about 1.3mm is clearly to observe. This has to be expected, since the CFD simulations are based on the assumption that at the wall all bubbles are of the size of the bubble departure diameter, which had been chosen to be constant and equal to this exact value. A smaller second peak corresponding to the coalescence of two such bubbles is present in the bubble size distribution as well. This behaviour is one more sign of the correct implementation of the coupling of the RPI wall boiling model and the MUSIG approach. Results at the second monitoring location (right diagram) converge nicely to a smooth bubble size distribution when the number of bubble size classes increases.

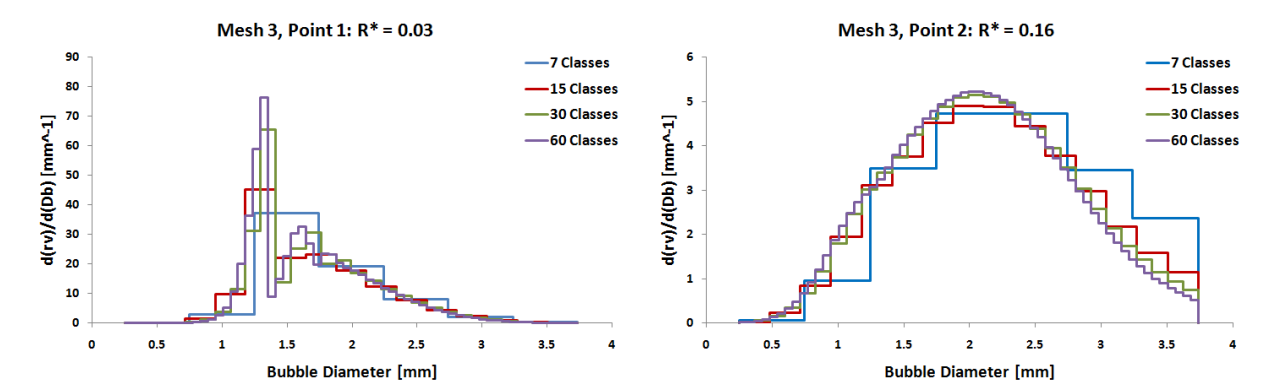


Figure 6. Investigation regarding independence of CFD solution from bubble size distribution discretization. Left: Bubble size distribution at Point 1. Right: Bubble size distribution at Point 2.

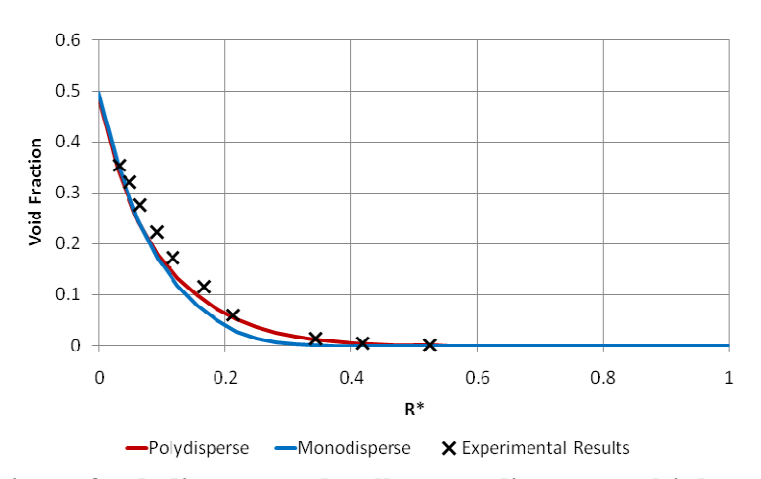


Figure 7. Comparison of polydisperse vs. locally-monodisperse multiphase flow predictions of R-113 boiling flow. Comparison of predicted steam volume fraction profiles to experimental data [1] at the measurement plane.

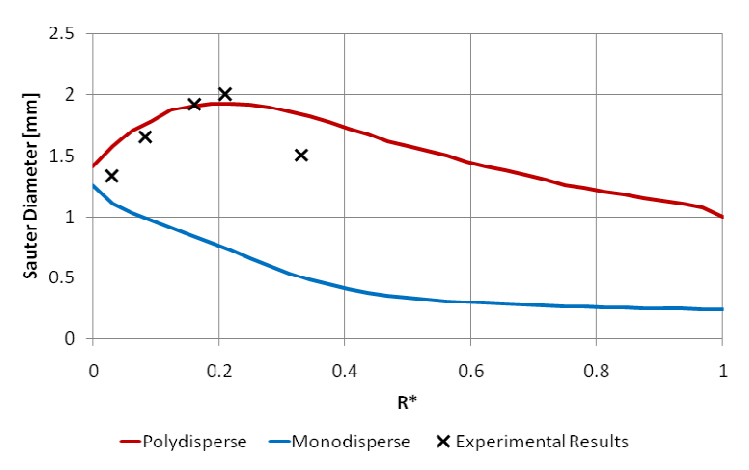


Figure 8. Comparison of polydisperse *vs.* locally-monodisperse multiphase flow predictions of R-113 boiling flow. Comparison of Sauter mean diameter to experimental data [1] at the measurement plane.

3.2.3 <u>Comparison of CFD Results with Homogeneous MUSIG Model and Locally-Monodispersed Wall Boiling Approach</u>

Finally, in order to investigate the improvement in modelling accuracy, we compared the CFD results as obtained from the coupled solution approach of RPI wall boiling model and homogeneous MUSIG model with the traditionally used approach of locally-monodispersed bubble diameter assumption in accordance to the correlation from eq. (2) by Kurul & Podowski [2]. From the previous studies it was considered as a fair compromise between established CFD solution accuracy and computational requirements to apply the spatial discretization corresponding to the Mesh 3 and the 15 classes bubble diameter discretization. Calculations were performed using the same physical setup as described before. In comparison the same CFD configuration but applying the traditional locally-monodispersed bulk bubble diameter approach was analyzed. The monodisperse results were obtained with the Kurul & Podowski correlation using a value of d_0 =0.15mm and d_1 =2mm in correspondence to eq. (2). Figures below show a direct comparison between the two approaches.

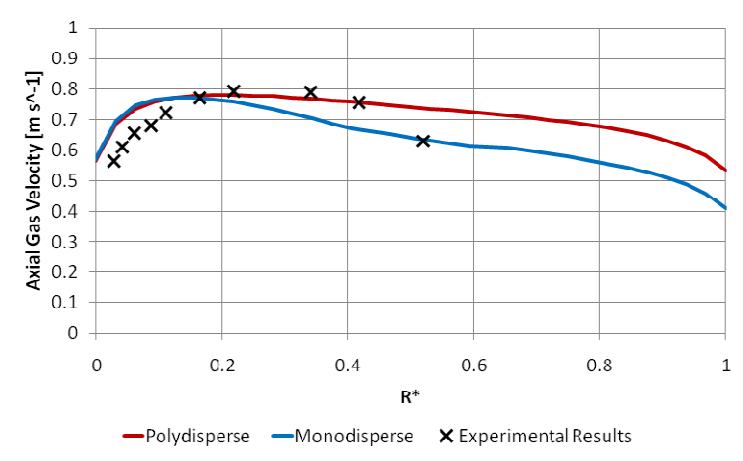


Figure 9. Comparison of polydisperse *vs.* locally-monodisperse multiphase flow predictions of R-113 boiling flow. Comparison of axial gas velocities to experimental data [1] at the measurement plane.

Figure 7 shows the radial steam volume fraction distributions predicted with both approaches. Both CFD simulations are able to reproduce the trend of the experimental values properly, however the profile corresponding to the polydisperse multiphase flow simulation is in slightly better agreement to data. A much larger sensitivity with regard to the approach used for the calculation of the bulk bubble diameter can be noticed in the radial profiles of the resulting Sauter mean diameter (Figure 8). By applying the new coupled approach based on homogeneous MUSIG model the results are now in a substantially better qualitative and quantitative agreement with data, i.e. showing the generation of steam bubbles at the wall corresponding to the size of the departure diameter followed by strong coalescence of steam bubbles at a radial position slightly shifted towards the center of the circular annulus and finally their collapse due to recondensation when the steam is in contact with the sub-cooled liquid. The quantitative agreement is very satisfactory. In contrary the locally-monodisperse approach can never reproduce the quantitative values or trends of the experiments for the measured Sauter mean diameter, showing an always decreasing bubble diameter increasing distance to the heated wall since in accordance with eq. (2) in this case the bulk bubble diameter is directly and linearly coupled with the local liquid subcooling and the effect of strong bubble coalescence in the near-wall area of high steam concentration cannot be reproduced.

Finally Figure 9 shows the comparison of the axial steam velocity. Both approaches are performing similar and slightly overpredict the measured velocity values in the near-wall region. But the consideration of a wall roughness proportional to the bubble departure diameter has still improved the agreement with data for both profiles in this region. However, at a position between $R^*=0.2$ to $R^*=0.4$ the CFD results from the polydisperse multiphase flow simulation exactly coincide with the experimental values, which is not the case of the results obtained by using the Kurul & Podowski correlation. This shows that the more exactly predicted Sauter mean diameter leads to a more exactly predicted steam bubble slip velocity with the continuous phase. For the outermost measurement point at $R^*=0.52$ it has be noted again, that the measurements at this location have to be regarded as non reliable, since the steam content at this position is rather

minor which should have led in the experiments to insufficient data rates and bad measurement statistics.

4. Conclusions

A new methodology to improve the accuracy of wall boiling simulations has been derived and implemented in a customised version of the CFD software package ANSYS CFX 12.1. It permits to substitute the Kurul & Podowski correlation for the bulk bubble diameter in the RPI model by application of a discrete population balance approach (homogeneous or inhomogeneous MUSIG model). In this way, a detailed size bubble distribution is computed at each bulk domain location, taking into account steam bubble breakup, coalescence and change of bubble size distribution due to evaporation and condensation. This in turn allows a more accurate prediction of the interfacial area density, which is the most influential parameter in all interfacial mass, momentum and heat transfer processes.

An investigation based on the CFD best practice guidelines has been carried out with regard to the spatial discretization and the discretization of the bubble size distribution into MUSIG bubble size classes. Almost mesh converged solutions could be obtained for Mesh 3. Furthermore it could be shown, that the CFD solution with the newly developed coupled approach of RPI wall boiling model and homogeneous MUSIG model becomes independent from the number of used MUSIG bubble size classes if more than about 15-20 size classes are used.

The improved solution algorithm has been compared to results from the traditionally used locally-monodispersed bulk bubble diameter assumption. The comparison for the test case of Roy et al. [1] shows an improved agreement of the CFD results from the homogeneous MUSIG model predictions with data, especially for the profiles of mean Sauter diameter and axial gas velocities.

5. Acknowledgements



This research has been supported by the German Ministry of Education and Research (BMBF, Grant No. 02NUK010G) in the framework of the R&D funding concept of BMBF "Basic Research Energy 2020+", the German CFD Network on Nuclear Reactor Safety Research and the Alliance for Competence in Nuclear Technology, Germany.

6. References

- [1] R.P. Roy, S. Kang, J.A. Zarate, and A. Laporta, "Turbulent subcooled boiling flow Experiments and simulations," *Journal of Heat Transfer*, vol. 124, no. February 2002, pp. 73-93, 2002.
- [2] N. Kurul and M.Z. Podowski, "On the modeling of multidimensional effects in boiling channels," <u>Proceedings of the 27th National Heat Transfer Conference</u>, Minneapolis, July 1991.
- [3] G. H. Yeoh and J. Y. Tu, *Modelling subcooled boiling flows*.: Nova Science Publishers, 2009.

- [4] Th. Frank, P. J. Zwart, E. Krepper, H.-M. Prasser, and D. Lucas, "Validation of CFD models for mono- and polydisperse air-water two-phase flows in pipes," *J. Nuclear Engineering & Design (NED)*, vol. 238, pp. 647-659, March 2008.
- [5] ANSYS, ANSYS CFX 12 Theory users manual. Canonsburg, USA: Ansys Inc., 2009.
- [6] Th. Frank, P. Beckstein, C. Lifante, and A. D. Burns, "Prediction of Subcooled Wall Boiling in a Heated Annulus Including Conjugate Heat Transfer in the Central Heated Rod," <u>Proceedings of the 7th International Conference on Multiphase Flow, ICMF 2010, May 30-June 4, 2010, Tampa, FL USA</u>, 2010, pp. 1-14.
- [7] V. I. Tolubisnki and D.M. Kostanchuk, "Vapour bubbles growth rate and heat transfer intensity at subcooled water boiling," <u>Proceedings of the 4th International Heat Transfer Conference</u>, Paris, 1970.
- [8] C. Lifante, T. Frank, A.D. Burns, D. Lucas, and E. Krepper, "Prediction of Polydisperse Steam Bubble Condensation in Sub-Cooled Water using the Inhomogeneous MUSIG Model.," <u>Proceedings of the 7th International Conference on Multiphase Flow</u>, Tampa, FL, 2010.
- [9] NIST Reference Fluid Thermodynamic and Transport Properties Database (REFPROP): Version 9.0. [Online]. http://www.nist.gov/srd/nist23.cfm
- [10] F.R. Menter, "Two-equation eddy-viscosity turbulence models for engineering applications," *AIAA Journal*, vol. 32, no. 8, pp. 1598 1605, 1994.
- [11] E. Krepper, D. Lucas, and M. Schmidtke, "Modelling of Turbulence in Bubbly Flows," <u>Proceedings of the 7th International Conference on Multiphase Flow</u>, Tampa, 2010.
- [12] A. Tomiyama, "Progress in computational bubble dynamics," <u>Proceedings of the Workshop on Multiphase Flows 2009</u>, Dresden, 2009.
- [13] B. Koncar and E. Krepper, "CFD simulation of convective flow boiling of refrigerant in a vertical annulus," *Nuclear Engineering and Design*, vol. 238, pp. 693-706, 2008.
- [14] V. I. Tolubinski and D.M. Kostanchuk, "Vapour bubbles growth rate and heat transfer intensity at subcooled water boiling," <u>Proceedings of the 4th International Heat Transfer</u> Conference, Paris, 1970.
- [15] F.R. Menter, "CFD Best Practice Guidelines for CFD Code Validation for Reactor-Safety Applications," 2002.
- [16] H. Anglart, O. Nylund, N. Kurul, and M. Z. Podowski, "CFD prediction of flow and phase distribution in fuel assemblies with spacers," <u>Proceedings of the NURETH-7, Saratoga Springs, New York</u>, 1995, Published in: Nuclear Eng. & Design (NED), Vol. 177 (1997), pp. 215-228.